J. Fluid Mech. (1996), vol. 320, pp. 211–233

Resonant growth of three-dimensional modes in Falkner–Skan boundary layers with adverse pressure gradients

By T. C. CORKE[1] AND S. GRUBER[2]

[1] Fluid Dynamics Research Center, Mechanical and Aerospace Engineering Department, Illinois Institute of Technology, Chicago, IL 60616, USA
[2] University of Stuttgart, Germany

(Received 25 April 1995 and in revised form 22 March 1996)

This work documents the spatial development of a triad of instability waves consisting of a plane TS mode and a pair of oblique modes with equal-opposite wave angles which are undergoing subharmonic transition in Falkner–Skan boundary layers with adverse pressure gradients. The motivation for this study is that for wings with zero or moderate sweep angles, transition is most likely to occur in the adverse pressure gradient region past the maximum thickness point and, starting with low initial amplitudes, subharmonic mode transition is expected to be the predominant mechanism for the first growth of of three-dimensional modes. The experiment follows that of Corke & Mangano (1989) in which the disturbances to produce the triad of waves are introduced by a spanwise array of heating wires located near Branch I. The initial conditions are carefully controlled. These include the initial amplitudes, frequencies, relative phase and oblique wave angles. The basic flow consisted of a Falkner–Skan (Hartree) boundary layer with a dimensionless pressure gradient parameter in the range $-0.06 \leqslant \beta_H \leqslant -0.09$. The frequency of the TS wave was selected to be near the most amplified based on linear theory. The frequency of the oblique waves was the subharmonic of the TS frequency. The oblique wave angles were set to give the largest secondary growth ($\approx 60°$). Compared to similar conditions in a Blasius boundary layer, the adverse pressure gradient was observed to lead to an extra rapid growth of the two- and three-dimensional modes. In this there was a relatively larger maximum amplitude of the fundamental mode and considerably shortened amplitude saturation region compared to zero pressure gradient cases. Analysis of these results includes frequency spectra, the wall-normal distributions of each mode amplitude, and mean velocity profiles. Finally, the streamwise amplitude development is compared with the amplitude model from the nonlinear critical layer analysis of Goldstein & Lee (1992).

1. Background

The basic understanding and accurate prediction of transition from laminar to turbulent flow in viscous boundary layers are of great practical interest. Transition in a decelerated flow field (with an adverse pressure gradient) is especially relevant to airfoils which are not highly swept. In these cases the dominant linear mode is expected to be Tollmien–Schlichting (TS), and transition is expected to only occur in the adverse pressure gradient region which occurs past the maximum thickness point.

Because of the multitude of known and unknown effects of external disturbances, the development of a general theory of transition is still far from complete. For instance, the empirical e^N-method (Van Ingen 1956) is still the standard tool in engineering practice, although it is known to ignore essential factors of the physics of transition, such as the initial amplitudes of disturbances, parametric interactions and nonlinear stages, and therefore may be misleading if used beyond the supporting data base.

The motivation for studying the transition process comes from the need to predict if and where transition occurs. Whether hypersonic vehicles can fly will be determined to a large extent by the accurate prediction of transition. Moreover, by controlling the state of the boundary layer, the performance of aircraft, particularly with respect to range and economy of operation, can be increased significantly.

Experiments on boundary layer transition conducted in low-disturbance wind tunnels have established three basic stages. Transition starts with the growth of the most amplified modes (wavenumbers and frequencies) predicted from linear stability theory. In a two-dimensional boundary layer over an essentially flat surface, these modes are TS waves. The frequencies and growth rates of these waves, which constitute the initial stage of linear instability, are predicted from the Orr–Sommerfeld equation for temporally growing disturbances in a locally parallel flow. In the second stage, three-dimensional spatially periodic instability modes appear. Starting with low initial amplitudes, the most likely three-dimensional modes are produced by a subharmonic resonance with the initial TS wave. This produces staggered Λ-shaped features in the unsteady vorticity field, with a spanwise wavelength which corresponds to an initial pair of oblique modes with equal-opposite wave angles. The third stage involves the generation of other nonlinear modes, which are derived from sum and difference interactions of the initial resonant modes. Included in this is a three-dimensional mode at the initial TS frequency, and a spanwise-periodic distortion of the mean flow.

The roots to understanding subharmonic transition in Blasius boundary layers comes from the theoretical work of Craik (1971) and Herbert (1983), and experiments by Kachanov, Koslov & Levchenko (1977), Kachanov & Levchenko (1984) Kachanov (1987), Saric & Thomas (1984), and Corke & Mangano (1989). Corke & Mangano were the first to simultaneously introduce a plane TS wave and a pair of oblique waves to directly set up a triad resonance. Starting with low initial amplitudes, they investigated three conditions of oblique waves with spanwise wavenumbers: one which satisfied Craik's model, and the other two which could only lead to resonance by the Herbert mechanism. By means of detailed hot-wire velocity surveys and smoke-wire flow visualization, they measured the amplitude and phase distributions in three space dimensions and documented the staggered peak–valley Λ-structures. The maximum amplification rates and spanwise wavenumbers were found to closely agree with the theoretical predictions of Herbert & Bertolotti (1985).

Recently, Goldstein & Lee (1992) have developed a nonlinear theory for a resonant triad of inviscid Rayleigh waves in an adverse pressure gradient boundary layer. In their analysis, the initial interaction is parametric. However, once oblique mode amplitudes become sufficiently large, the resulting growth rates of the triad modes become fully coupled, and nonlinear interactions have a dominant effect. The nonlinear interactions include a cubic self-interaction of the oblique modes, cubic mutual interaction of the three-dimensional mode with the two-dimensional mode, and a quartic back interaction of the three-dimensional mode onto the two-dimensional mode. The analysis of Goldstein & Lee was the first to consider coupled amplitude equations of this type.

Following the approach of Goldstein & Lee, Mankbadi, Wu & Lee (1993) analyzed

the zero pressure gradient (Blasius) boundary layer in the quasi-equilibrium limit. Here, the fully nonlinear interactions of a triad of instability waves are considered in a matched asymptotic expansion in their nearly common viscous critical layers. The expansion was done for conditions in the vicinity of the upper branch of the linear stability neutral curve. In this work, there is no back-reaction effect on the two-dimensional wave at the lowest order. The analysis revealed a double-exponential growth of the oblique waves with resonance. During this stage, the plane wave continues to follow linear theory. When the amplitude of the oblique waves exceeds that of the plane wave by a certain amount, a nonlinear stage comes into effect in which the self-interaction of the oblique waves becomes important. This was found to lead to an oscillatory amplitude saturation stage.

More recently, Lee (1994) extended the inviscid analysis of Goldstein & Lee to include viscous effects and a generalized scaling. His analysis was shown to be valid for Falkner–Skan boundary layers without (Blasius) and with pressure gradients. He found that his $\mathcal{O}(1)$-viscosity solution approached the viscous limit solution of Mankbadi *et al.* (1993) as viscosity became large. A primary focus of Lee's work is on the quartic back-reaction term in the Goldstein & Lee analysis. As opposed to the oscillatory saturation that occurs in the quasi-equilibrium conditions of Mankbadi *et al.* (1993), this term produces faster-than-exponential growth of the parametric resonance stage and ultimately a singularity at a finite downstream position.

In addition to Goldstein & Lee (1992) and Lee (1994), the influence of pressure gradients on resonant-triad evolution has been studied by Zelman & Maslennikova (1993*a*,*b*) and Herbert & Bertolotti (1985). Zelman & Maslennikova used a first-order weakly nonlinear stability analysis of a triad of TS waves. The work of Herbert & Bertolotti follows the approach of Herbert (1983) and involves the secondary instability of a basic flow consisting of the mean flow and a plane TS wave to three-dimensional Squire modes. All these are applicable to the parametric resonance development region which governs the enhanced growth of the subharmonic three-dimensional mode.

Kloker & Fasel (1990) and Kloker (1993) performed a fully nonlinear direct Navier–Stokes spatial calculation for Falkner–Skan boundary layers. In most of their calculations, they used a large adverse pressure gradient which was close to separation ($\beta_H = -0.18$). Their input disturbances consisted of a plane wave ($F \times 10^6 = 108$) and pair of oblique waves at the subharmonic frequency. With this they were able to follow the development into the nonlinear stage which included the generation of interacted (sum and difference) modes and energy saturation.

1.1. *Objective*

In this paper we experimentally investigate the effect of mild adverse pressure gradients on subharmonic mode transition. For this we utilize the setup of Corke & Mangano (1989) in which periodic disturbances are introduced to excite a resonant triad with known initial amplitudes, frequencies, and oblique-mode wave angles. The streamwise development of these modes will be documented through their linear, parametric and fully coupled stages so that it can be compared to a general coupled amplitude model which follows that of Goldstein & Lee (1992).

2. Experimental setup

The experiment was performed in the IIT Boundary Layer Stability Wind Tunnel which has been exclusively developed for conducting experiments on instability and

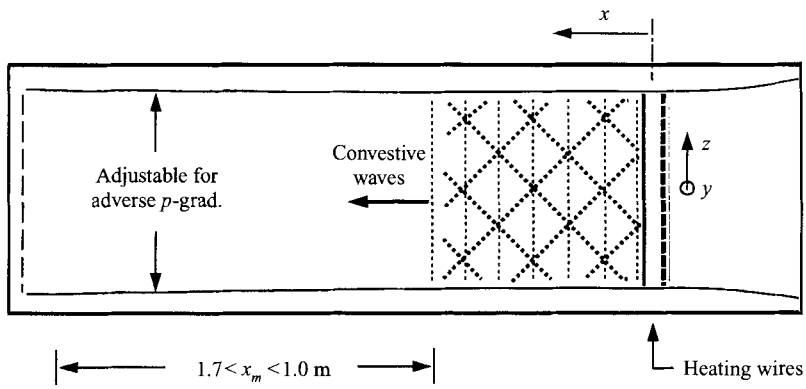

FIGURE 1. Schematic of measurement section showing location of heating wire array and movable panels for pressure gradient control.

transition in Blasius boundary layers using computer-controlled mode forcing and data acquisition. All the documentation of the wind tunnel is presented by Corke & Mangano (1989).

The wind tunnel is a low-speed, low-disturbance, open-circuit type which is well suited for boundary layer transition experiments. A schematic of the wind tunnel measurement section is shown in figure 1. The turbulence intensity (u'/U_∞) in the test section is approximately 0.07%. The measurement section is rectangular in cross-section with dimensions of 73.7 cm high by 15.25 cm deep by 2.46 m long. The boundary layer develops on the back wall of the test section, which consists of a stainless steel surface bonded to a honeycomb composite. The surface is flat and has a nearly optical-mirror finish. Access with hot wires is made through 15 slots in a clear Plexiglas panel which forms the front wall of the measurement section. The slots are positioned 102, 118, 134, 138, 143, 147, 155, 162 and 170 cm downstream of the heating wire array. Each slot has a removable insert which provides a smooth flush inside surface when not in use. Rubber strips are used to seal any gap around the hot-wire probe body.

The test section is subdivided into three regions by top and bottom panels. The smaller top and bottom regions are at a slightly lower pressure than the middle measurement region. The pressure difference is set up by a perforated grid at the end of the middle section. A small gap in the junction of the top and bottom panels and the back wall is adjusted to draw off fluid and prevent the destabilization of the three-dimensional corner flow.

Different streamwise pressure gradients were set by moving the top and bottom panels to increase or decrease the cross-sectional area of the middle measurement region. In this experiment, two adverse pressure gradients ($dp/dx > 0$) corresponding Falkner–Skan (Hartree) parameters $\beta_H = -0.06$ and $\beta_H = -0.09$ were used. These relatively small pressure gradients were chosen to provide a long enough region to measure what was expected to be an 'explosive' growth of the subharmonic mode. The pressure gradient was applied in the downstream half of the measurement section. Figure 2 shows a comparison between the theoretical and measured free-stream velocity for the two pressure gradients.

The panels in the upstream half of the measurement section were adjusted to produce a zero pressure gradient ($\beta_H = 0$). This was in the region of Branch I, where the heating wires were located. The advantage of a zero pressure gradient

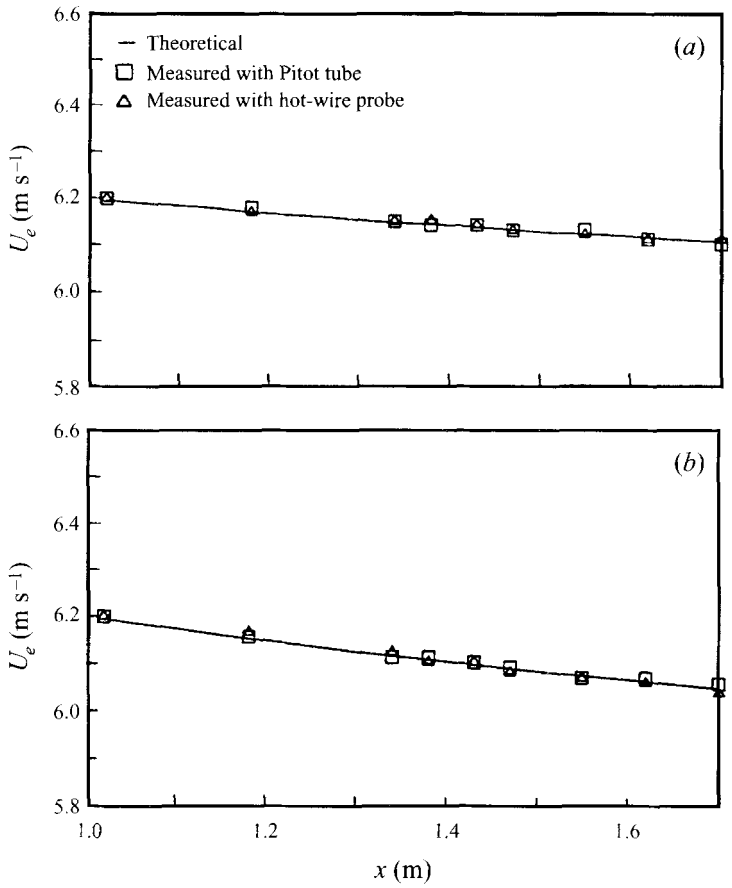

FIGURE 2. Free-stream velocity distribution in measurement section for (*a*) $\beta_H = -0.06$ and (*b*) $\beta_H = -0.09$. Free-stream velocity $U_\infty = 6.2$ m s^{-1}.

in this region was to provide an initial slower, more controlled growth of the input disturbances into the region of the measurement slots. It also allowed some cross-checks to the previous experiments such as Corke & Mangano (1989), Korategere (1990) and Hsia (1993) which were performed in this facility with zero pressure gradient.

As with our earlier experiments, we introduce both two- and three-dimensional disturbances into the boundary layer in order to excite a plane TS wave and oblique wave pairs. This is achieved using a spanwise array of 0.05 mm diameter heating wires which are suspended at the height of the critical layer, at the streamwise location just upstream of the lower linear stability neutral branch (based on a Blasius flow). The wires are periodically heated to introduce controlled perturbations through local changes in the air viscosity. Corke & Mangano (1989) showed that this is analogous to a wall-normal velocity perturbation. Each heating wire is individually controlled to allow a spanwise phase change between adjacent wires. Changing the phase allows different oblique wave angles. The plane (two-dimensional) wave is introduced using a separate single wire which spans the full width of the measurement section. This is located upstream of the short-wire segments. The amplitude, frequency and phase of the periodic signal to the single (two-dimensional) wire are controlled separately from the three-dimensional wire segments. This allows us to independently change

Case	β_H	R_x	U_e (m s^{-1})	$F \times 10^6$ 2D:3D	A_{2D} (V)	x_v (cm)
2-D	−0.06	523–734	6.196–6.105	96: –	26	+34
2-D	−0.06	523–734	6.196–6.105	96: –	32	+34
2-D	−0.09	503–718	6.195–6.060	96: –	30	+39
0	−0.06	523–734	6.196–6.105	96:48	26	+34
1	−0.06	523–734	6.196–6.105	96:48	32	+34
2	−0.09	503–718	6.195–6.060	96:48	30	+39

TABLE 1. Experimental conditions.

the initial conditions to the two- and three-dimensional disturbances. Further details of the method are contained in the paper by Corke & Mangano (1989).

A list of experimental conditions is contained in table 1. These were divided into six cases. In three of these (Cases 2-D) only a plane TS mode was excited. These were primarily used to make comparisons to linear stability theory. The other three cases correspond to when the two- and three-dimensional modes were combined. In two of these (1 and 2), they differed only in the initial amplitude of the two-dimensional mode. In table 1, $F = 2\pi f v/U_\infty^2$, where f is the physical frequency, $R_x = (U_\infty x/v)^{1/2}$, where x is measured from x_v and x_v is the x-location of the Falkner–Skan virtual leading edge, and A_{2D} is a reference voltage supplied to the two-dimensional heating wire.

2.1. *Instrumentation and processing*

A single hot-wire sensor, which was mounted on a motorized traversing mechanism, was used to measure the streamwise velocity component. The hot wire was operated in a constant-temperature mode. The voltage time series proportional to velocity was split into two parts and acquired through an A/D of a digital acquisition and control (DAC) computer. One part of the analog signal contained the d.c. part. This was d.c. biased and amplified by a fixed gain. The other analog signal had the d.c. removed by an analog band-pass filter which was set to high pass at 1.0 Hz and low pass at 100 Hz. The latter was to prevent frequency aliasing. The a.c.-containing signal was then passed through a computer-controlled programmable gain circuit. During acquisition, the gain was varied to maintain the highest possible resolution through the A/D. The time series were added back together in the computer using floating-point accuracy.

The data series typically consisted of 16 records of contiguous samples at discrete y-positions making up a profile in the wall-normal direction. Each record contained 512 samples acquired at 6 times the fundamental mode frequency. A profile would typically consist of 25–30 wall-normal positions, with the greater concentration of points occurring in regions of large gradients.

The spanwise (z) centreline was measured with respect to the location of the standing pattern of oblique mode crossings. Then $z = 0$ corresponded to the intersection of pair of oblique waves, which also corresponded to the spanwise location of the subharmonic mode amplitude maximum.

The time series processing consisted of computing the time-averaged velocity, as well as obtaining frequency information from FFT-based spectra. The amplitudes corresponding to spectral peaks were converted to r.m.s. by taking the areas under the peaks and normalizing them by the frequency band width. Because the instability modes were input by the same computer that acquired the time series, a common

phase reference existed. Therefore data series taken at a different points in space and time could be related to each other. This allowed us to compute phase velocities and streamwise wavelengths for the instability modes.

3. Results

3.1. *Basic flow*

Because the measurement wall for the experiment was the back wall of the tunnel test section, there was no physical leading edge to define a virtual origin, x_v, for the boundary layer growth. Any comparisons to a Falkner–Skan mean flow development (and stability Reynolds number) then required the use of a reference location, referred to as the virtual leading edge. The location of the virtual leading edge was determined from the displacement thickness of the assumed Falkner–Skan boundary layer, given as

$$\delta_1(x) = D_1[(2-\beta_H)(xv/U_e)]^{1/2} \tag{3.1}$$

where

$$U_e(x) = U_\infty x^m, \quad m = \beta_H/(2-\beta_H) \tag{3.2}$$

and

$$D_1 = \int_0^\infty (1-f'(\eta))\mathrm{d}\eta \tag{3.3}$$

where f' and η refer to the Falkner–Skan mean velocity and similarity wall-normal distance, respectively. When $\beta_H = -0.06$, $D_1 = 1.33497$, and

$$\delta_{1_{calc}} = 1.916[(x-x_v)v/U_e)]^{1/2}. \tag{3.4}$$

When $\beta_H = -0.09$, $D_1 = 1.41265$, and

$$\delta_{1_{calc}} = 2.042[(x-x_v)v/U_e)]^{1/2}. \tag{3.5}$$

Mean velocity profiles were measured on the spanwise centreline, at the different streamwise positions from $x = 1.02$ to 1.38 m, for all the experimental conditions: unforced, two-dimensional only, and two- and three-dimensional combined. These were integrated to determine $\delta_1(x)$. For a known $U_e(x)$ with each β_H, values of $\delta_{1_{calc}}(x)$ were compared to the measured $\delta_1(x)$ while varying x_v in an iterative process to minimize the least-squared error. The result for $\beta_H = -0.06$ was $x_v = 34$ cm (downstream of the heating wires). For $\beta_H = -0.09$ the value was $x_v = 39$ cm. For both pressure gradients, the largest standard deviation between the measured streamwise development of δ_1 and the theoretical development using these values of x_v, was less than 6%.

The streamwise variation in δ_1 and the shape factor $H_{12} = \delta_1/\delta_2$ are shown in figure 3 for the case with $\beta = -0.06$. This pressure gradient gave the larger standard deviation, so that it represents the worst case in determining x_v. The solid line corresponds to the theoretical variation, using the estimated value for x_v. The small deviation that occurs for $x > 1.43$ m is due to mean flow distortion when the modes grow to large amplitudes. The corresponding mean velocity profiles for the more downstream x-locations are shown in figure 4. Here we observe a good collapse of the data onto the theoretical profile until the last x-position where the strong mean flow distortion is evident.

3.2. *Periodic mode development*

The conditions for the experiment are summarized with respect to the neutral linear-stability curves for the Falkner–Skan boundary layers in figure 5. The two curves

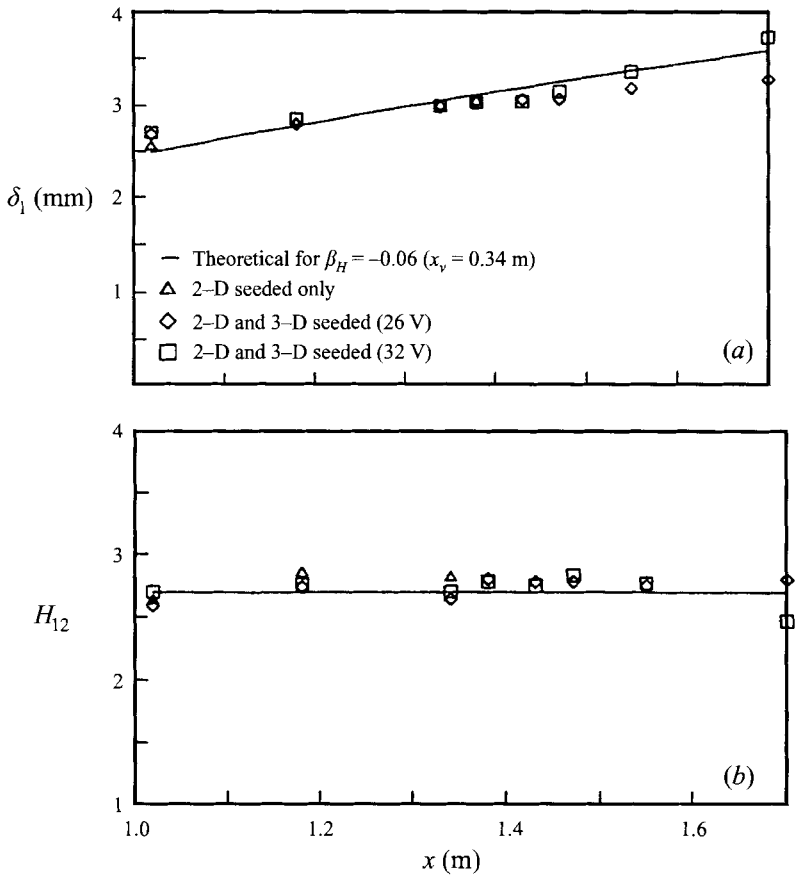

FIGURE 3. Comparison of similarity quantities for Case 1: (*a*) δ_1 and (*b*) H_{12}.

correspond to the two values of β_H. The frequency of the plane TS wave used in the experiment corresponded to a dimensionless value of $F \times 10^6 = 96$. This is indicated by the dashed line in the figure. Also indicated are the respective locations of the heating wires, and the streamwise bounds of the hot-wire surveys.

Figure 6 shows velocity spectra in the wall-normal (y) direction at the most-upstream location ($x = 1.02$ m) with $\beta_H = -0.06$. This is representative of all the spectra, showing clear peaks corresponding to the fundamental (TS) mode at 38 Hz and the subharmonic three-dimensional mode at 19 Hz. The amplitude distributions in the wall normal direction of the two modes are taken from spectra such as these.

A sensitive secondary check of the basic flow comes by comparing the amplification rate and streamwise wavenumber of the two-dimensional TS mode in the cases when it was the only mode seeded. Figure 7(*a*) shows the growth in maximum amplitude of this mode for two initial amplitudes in the boundary layer with $\beta_H = -0.06$. For these, the natural log of the amplitude was taken to highlight exponential growth. The slope corresponds to the dimensional streamwise amplification rate, $\alpha_i = 1.7\ \mathrm{m}^{-1}$. Signifying the linear regime in the two cases, the change in initial amplitude only shifted the curve, with the slope remaining the same.

The streamwise wavenumber, α_r, was derived from the downstream change in the mode phase, such as shown in figure 7(*b*) (details on the general determination of α_r and α_i from data such as these are given by Corke & Mangano 1989, §6.2).

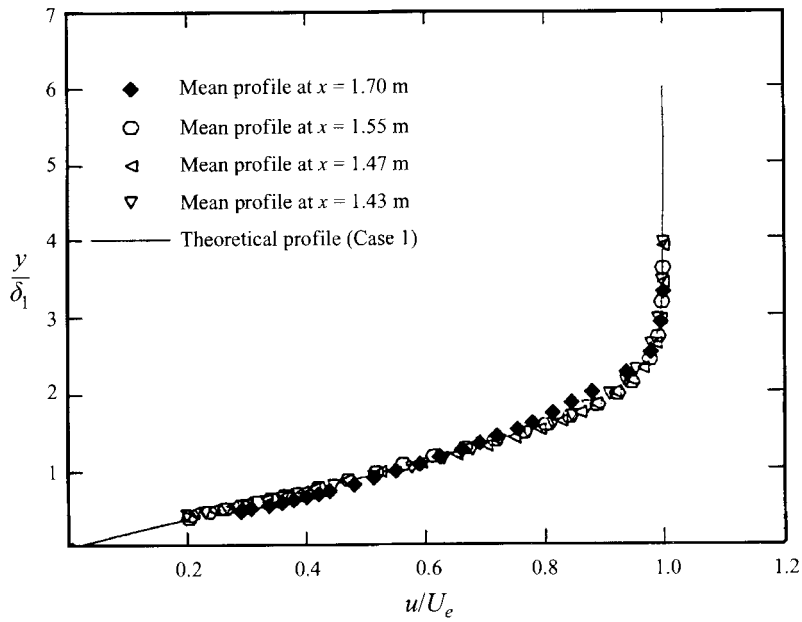

FIGURE 4. Mean velocity profiles at different downstream locations for Case 1.

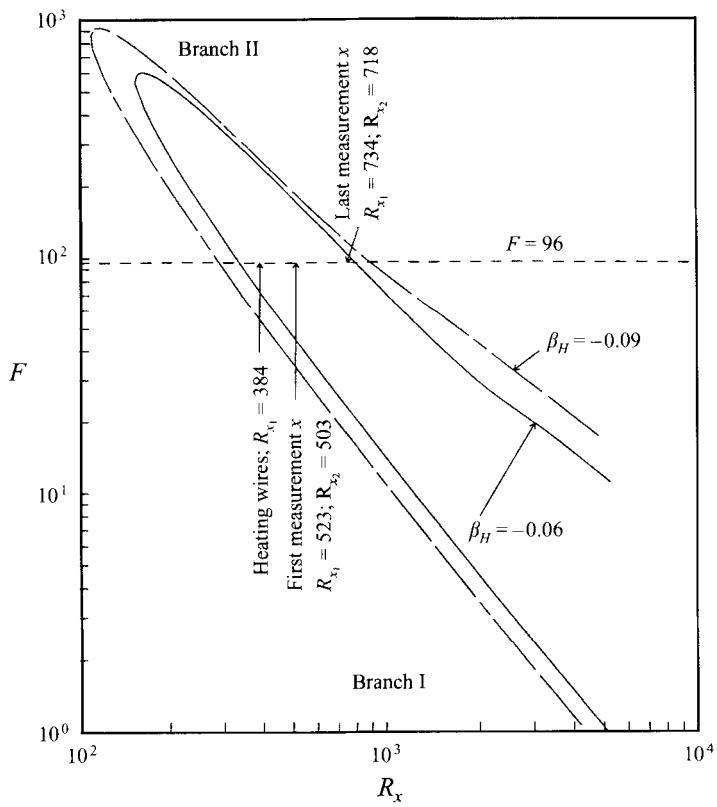

FIGURE 5. Measurement locations with respect to neutral linear-stability curves for $\beta_H = -0.06$ and -0.09. Subscripts 1 and 2 on R_x refer to Cases 1 and 2.

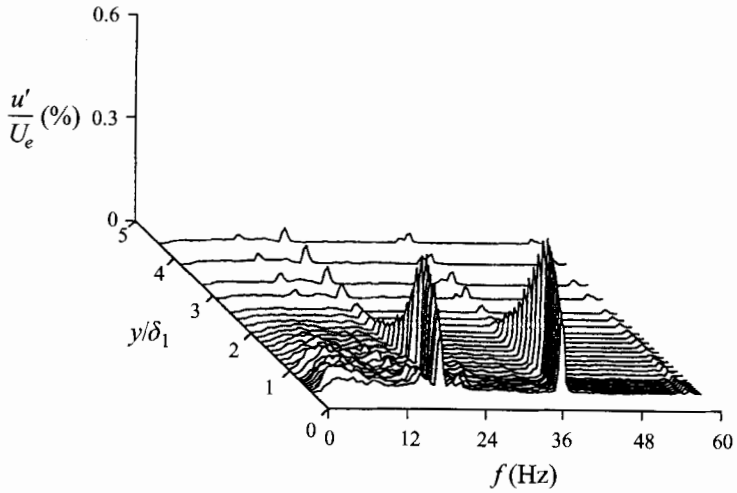

FIGURE 6. Representative spectra at different wall-normal positions in the boundary layer, taken here at the most-upstream measurement location in Case 1.

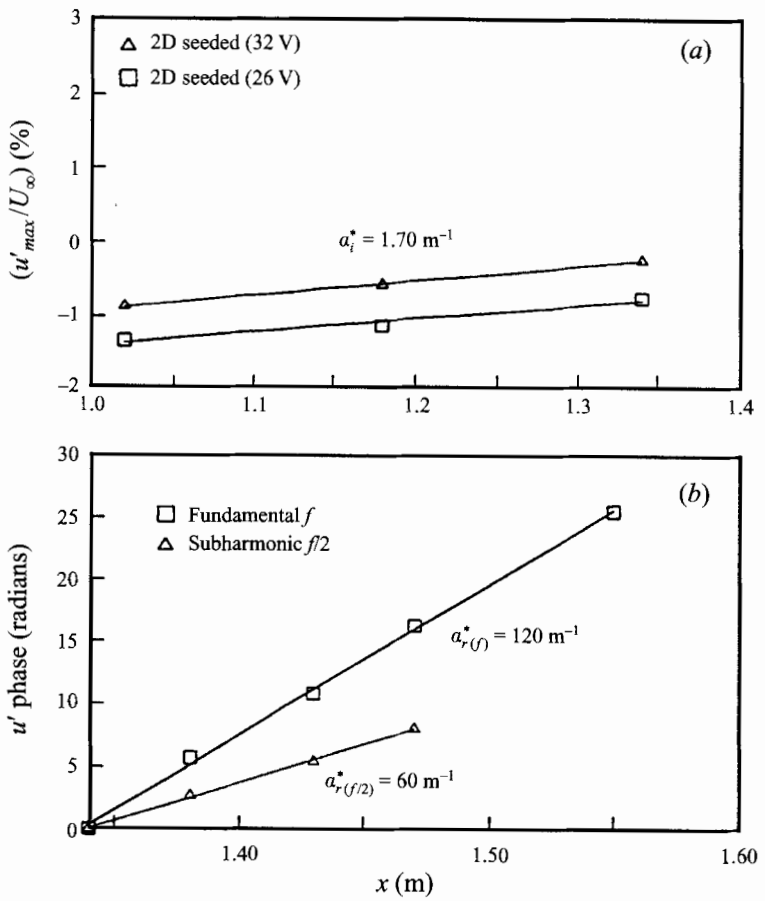

FIGURE 7. Streamwise development of amplitude (*a*) and phase (*b*) which were used to determine the linear amplification rate and streamwise wavenumber. $\beta_H = -0.06$; (*a*) $\alpha_i = 0.0022$, $f = 38$ Hz; (*b*) $\alpha_r = 0.1628$, $f = 38$ Hz, 26 V.

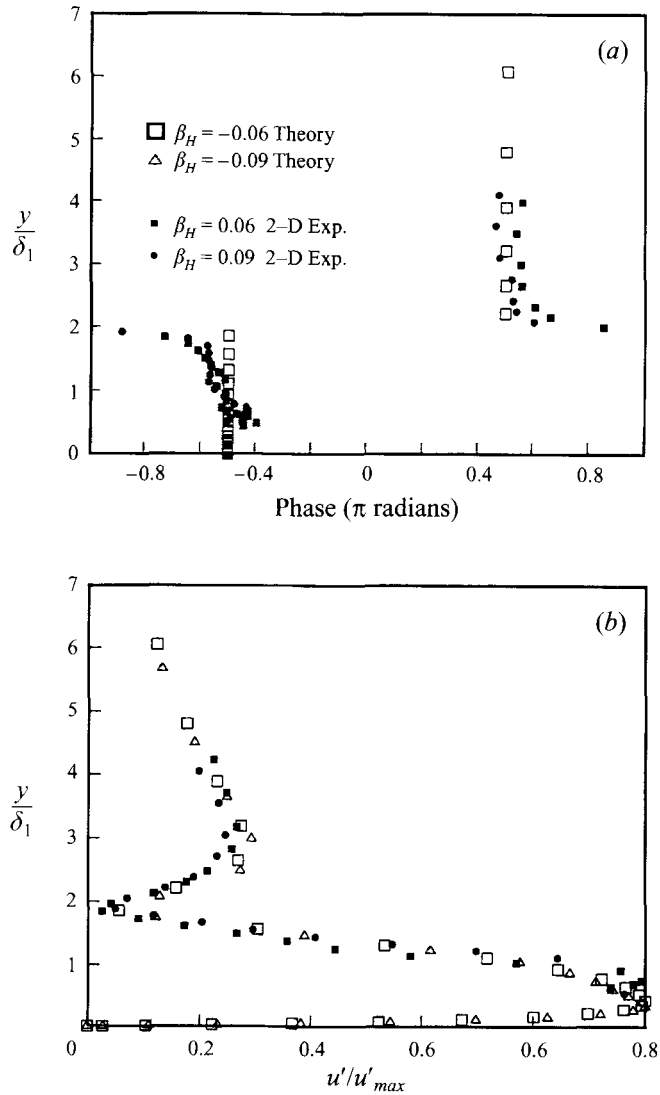

FIGURE 8. Wall-normal distributions of phase (*a*) and amplitude (*b*) for plane TS mode at the two pressure gradients. Open symbols correspond to Orr–Sommerfeld eigenfunction. Closed symbols correspond to measured data. $\alpha_r = 0.1559, \alpha_i = 0.0022$.

These correspond to the two- and three-dimensional modes in combination in Case 0. The square symbols denote the phase development for the plane TS mode. The triangle symbols correspond to the subharmonic three-dimensional mode. These show a constant streamwise wavenumber for the two modes over the region of measurement, with the ratio between two- and three-dimensional being 2:1 as required for subharmonic resonance.

In terms of the plane TS mode, the combination of their dimensionless wavenumbers $\alpha_i = 0.0022$ and $\alpha_r = 0.1628$, is in excellent agreement with linear stability calculations at this position where $Re_x = 523$. We also found excellent agreement in terms of the eigenfunction modulus and phase. These are shown in figure 8. The open symbols correspond to the y-eigenfunction for the u-component for the two values

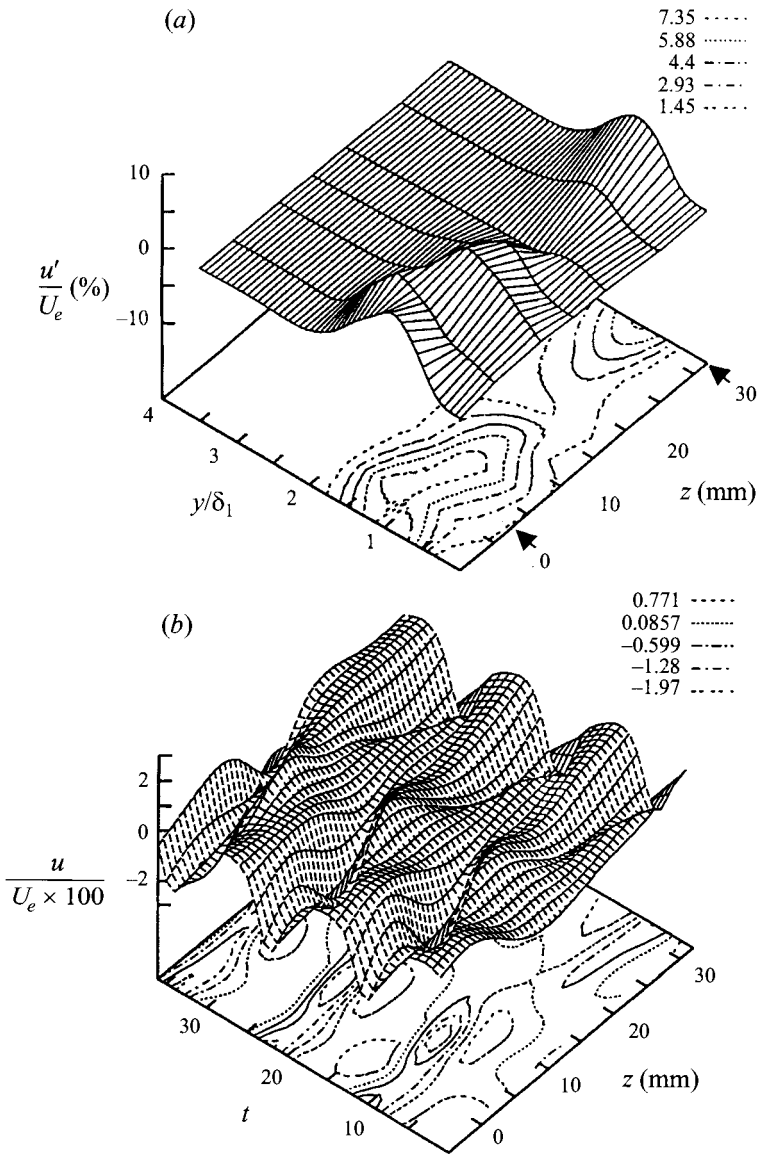

FIGURE 9. Spanwise distribution of wall-normal amplitude profile (*a*) and phase-averaged mean-removed velocity (*b*) for subharmonic three-dimensional mode at $x = 1.62$ m. Case 2, mode $f/2$.

of β_H used in the experiment. These were determined from a spectral calculation (Herbert 1990) of the Orr–Sommerfeld equation. The experimental points are shown as the filled symbols. These correspond to the most upstream measurement location. The amplitudes are normalized by the maximum value so that the shape of the eigenfunction can be compared. The comparison between the experiment and theory is excellent, signifying that both the mean and perturbation flows at the initial stages are in accordance with linear-amplitude theoretical predictions.

In the previous figures the documentation of the perturbation flow was in terms of the streamwise wavenumbers only. Figure 9 verifies the spanwise wavenumber

for the subharmonic mode. Figure 9(*a*) shows the amplitude distribution in the wall-normal direction at different spanwise (z) positions. These are shown both as a surface plot and as iso-amplitude contours. We chose to show this for Case 2 at a further downstream location ($x = 1.62$ m) because the larger amplitude there makes it easier to determine the spanwise locations of amplitude maxima. Twice the spanwise distance between amplitude maxima corresponds to the spanwise wavelength, λ_z, of the subharmonic mode. These are marked by the arrows in the figure. The streamwise wavenumber is $\beta = 2\pi/\lambda_z$. Our disturbance input was designed to introduce oblique waves with wave angles of $\theta = \pm 60°$. The spanwise wavelength is then $2\pi/(\alpha_r \tan(\theta))$. Using the dimensional $\alpha_{r_{f/2}}$ from figure 7(*a*), $\lambda_z/2 = 30.25$ mm. This agrees well with the spacing between the maxima in figure 9(*a*). Also, for oblique mode pairs, there should be a 180° phase shift between the locations of the two amplitude maxima. To verify this, figure 9(*b*) shows for the same x-location the phase-averaged velocity fluctuation at a fixed distance above the wall where the amplitude is a maximum, at different positions in the spanwise direction. This is shown as a surface plot and constant-level contours. From this we can see that at a fixed time in the cycle, for example $t = 20$, at the spanwise position of one maximum ($z = 2.5$ mm), we are at the top of the wave, whereas at the position of the other maximum ($z = 32$ mm) we are at the bottom of the wave, signifying a 180° phase difference. Therefore based on these, the conditions for the subharmonic three-dimensional mode have been verified.

The results to this point were intended to document the basic flow and the initial conditions for the input linear modes which would lead to subharmonic resonance. These were a necessary precursor to our main interest which was in the nonlinear streamwise development of these modes. The streamwise development of the maximum amplitude normalized by the local boundary layer edge velocity, U_e, is shown for the two pressure gradients in figure 10. The circle symbols correspond to the development of the plane TS mode when it was seeded by itself. The triangle and square symbols correspond to the plane TS and three-dimensional modes in combination. The solid curves through the points are intended only to guide the eye. In both figures 10(*a*) and 10(*b*), the initial amplitude of the two-dimensional mode, alone or with the three-dimensional mode, remained the same, although they were different for the two different pressure gradients (see table 1). For the three-dimensional mode, the z-location of the measurements corresponded to that of the subharmonic mode amplitude maximum at $z = 2.5$ mm such as was shown in figure 9(*a*). The general features we observe in the development of the two modes are:

(i) the rapid growth of the subharmonic mode, which according to linear theory is less amplified than the fundamental two-dimensional mode; and

(ii) the eventual larger-than-linear growth of the fundamental mode further downstream.

The first of these is due to a parametric resonance between the fundamental and subharmonic modes. The second is due to a back-interaction of the subharmonic mode with the fundamental which occurs when the subharmonic mode reaches a large amplitude.

In both cases, the initial amplitudes were comparable. The effect of the adverse pressure gradient was:

(i) to produce a more rapid growth of both modes;

(ii) to cause a greater overall amplitude of the fundamental mode compared to the subharmonic mode;

(iii) to significantly increase the amplitudes reached by both modes; and

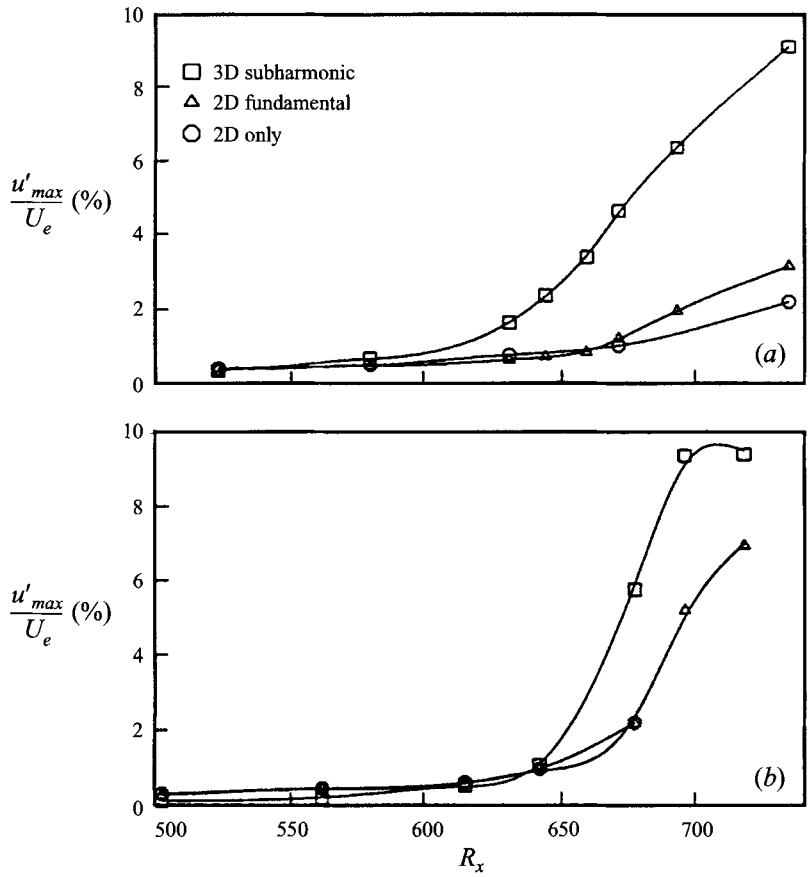

FIGURE 10. Streamwise development of maximum amplitude for two cases: (*a*) $\beta_H = -0.06$, Case Two-dimensional (32V) and Case 1; and (*b*) $\beta_H = -0.09$, Case Two-dimensional (30V) and Case 2.

(iv) to produce a relatively short (almost nonexistent) amplitude saturation region. With a zero pressure gradient case of comparable initial amplitudes (Corke & Mangano 1989), the maximum amplitude of the subharmonic mode only reached a value of 4.5% at amplitude saturation. In that case, the fundamental mode amplitude reached only 20% of the subharmonic mode amplitude. Also, there was a broad region where the amplitudes of both modes saturated and decayed. These features are in sharp contrast to the present results contained in figure 10.

3.3. *Amplitude model*

The most relevant model for subharmonic resonance in adverse pressure gradient boundary layers comes from Goldstein & Lee (1992). Others include the nonlinear model of Mankbadi (1990, 1991) and Mankbadi *et al.* (1993), which were derived for a Blasius layer, and the recent weakly nonlinear (linear-quadratic) model by Zelman & Maslennikova (1993*a*,*b*). Each of these has a parametric resonance leading to the initial growth of the subharmonic three-dimensional mode. The Goldstein & Lee and Mankbadi models also include a quartic dependence of the fundamental mode amplitude on the amplitude of the subharmonic.

Our goal was to use a general form of coupled amplitude equations in which we could determine coefficients by a least-square-error fit of the model to the experimental

results. We intended that these model equations contain the same physics as those developed by Goldstein & Lee (1992; equation 5.50). To achieve this, a convenient starting point was the form of the evolution equations given by Mankbadi (1991). These are in complex form,

$$\left.\begin{aligned}\frac{\mathrm{d}A}{\mathrm{d}R} &= \sigma^4(1+R_i^2/R^2)[(K_0+\mathrm{i}K_i)A+\mathrm{i}M_1(\mathscr{R}^{4.5}/\lambda^{1.5})ABB^* \\ &\quad -\mathrm{i}M_2(\mathscr{R}^6/\lambda^2 B^*B^3],\\ \frac{\mathrm{d}B}{\mathrm{d}R} &= \sigma^4(1+R_i^2/R^2)[K_{0b}B+0.3\pi(\mathscr{R}^3/\lambda)\mathrm{i}B^*A-0.4\mathrm{i}M(\mathscr{R}^{4.5}/\lambda^{1.5})B^2B^*]\end{aligned}\right\} \tag{3.6}$$

where A and B refer to the fundamental and subharmonic modes respectively. In (3.6), σ is a constant small-frequency parameter; $\mathscr{R}$ is a Reynolds number scaling parameter equal to $\sigma^{10}R$; R_i is an initial Reynolds number (equal to 523 in Case 1 and 503 in Case 2); K_0 and K_{0b} are the linear amplification rates; M_2 is a back-reaction coefficient and $M = M_r + \mathrm{i}M_i$ is a self-interaction coefficient, both of which are constant functions of the oblique wave angle θ; and λ is the skin friction coefficient.

These equations were simplified by: (i) noting that the subharmonic mode wave angles in the experiment were $\theta = 60°$, which leads to dropping the linear frequency detuning parameter, K_i, (ii) dropping the mutual interaction term, $\mathrm{i}M_1(\mathscr{R}^{4.5}/\lambda^{1.5})ABB^*$ in the equation for A (this was also dropped by Mankbadi *et al.* 1993) and (iii) choosing a subharmonic phase shift, $\phi_0 = 0$ and frequencies $\omega_1 = 2\omega_2$, which model the maximum growth.

Complex periodic functions were substituted for A, B and B^*, and the real and imaginary parts were separated. The equations for the real part are

$$\left.\begin{aligned}&\frac{\mathrm{d}|A|}{\mathrm{d}R} = \sigma^4(1+R_i^2/R^2)[(K_0|A| - M_2(\mathscr{R}^6/\lambda^2)|B|^4],\\ &\frac{\mathrm{d}|B|}{\mathrm{d}R} = \sigma^4(1+R_i^2/R^2)[K_{0b}|B| + 0.3\pi(\mathscr{R}^3/\lambda)|B||A| + 0.4M_i(\mathscr{R}^{4.5}/\lambda^{1.5})|B|^3],\\ &K_0 = \lambda^2/(2\sqrt{2}\mathscr{R}) - (\pi/8)(\mathscr{R}^2/\lambda^3),\\ &K_{0b} = [\lambda^2(\cos\theta)^{1/2}/\mathscr{R} - (\pi/8)(\mathscr{R}^2/\lambda^3\cos\theta)]/(\cos\theta + 1/\cos\theta).\end{aligned}\right\} \tag{3.7}$$

Equation (3.7) represent the amplitude envelope as a function of Reynolds number ($R = (U_e x/\nu)^{1/2}$) for the two modes. We write these in a general form as

$$\left.\begin{aligned}\frac{\mathrm{d}|A|}{\mathrm{d}R} &= (\overbrace{C_1 + C_2/R}^{\textit{linear}} + \overbrace{C_3R^2 + C_4/R^3}^{\textit{mean div.}})|A| + (C_5R^6 + C_6R^4)|B|^4,\\ \frac{\mathrm{d}|B|}{\mathrm{d}R} &= (C_7 + C_8/R + C_9R^2 + C_{10}/R^3)|B| + (C_{11}R + C_{12}R^3)|A||B|\\ &\quad - (C_{13}R^{2.5} + C_{14}R^{4.5}|B|^3.\end{aligned}\right\} \tag{3.8}$$

Here we see that the evolution of the fundamental mode amplitude, $|A|$, comes from its linear growth, which we denote as a combination of a linear part and a correction for divergence of the mean flow, and a quartic dependence on the subharmonic mode amplitude. The evolution of the subharmonic mode amplitude, $|B|$, comes from a linear growth, a parametric interaction with the fundamental mode, and a cubic self-interaction. This form is also very similar to that of Mankbadi *et al.* (1993). Comparing these equations to the amplitude equation of Goldstein & Lee (1992, equations 5.50 and 5.51) we see that they are also similar if we neglect the history effects. For example (following our notation), the amplitude development of the

two-dimensional mode involves a linear part (A) and a quartic interaction (B^4). They however had retained the mutual interaction term (B^2A) which we dropped. For the subharmonic mode, we both have the linear growth (B), parametric interaction (AB) and the cubic self-interaction (B^3) terms.

Our method was to determine C_i, $i = 1,\ldots,14$, by a least-squares fit of the maximum normalized amplitudes of the fundamental and subharmonic modes with R. For this, a cubic-spline fit to the experimental amplitude evolution was used to determine $\mathrm{d}|A|/\mathrm{d}R$ and $\mathrm{d}|B|/\mathrm{d}R$. Having determined the best fit of the model to the experimental data, the coupled amplitude equations were numerically integrated using a second-order backward-Euler method with a variable-step-size algorithm to maintain an error $< 10^{-6}$. The use of an implicit method for integrating the equations was found to be necessary because of their stiff nature. The integration was started at the conditions of the most-upstream measurement location.

The comparison of the model to the amplitude development with $\beta = -0.06$, Case 1, is shown in figure 11(a). The original data are shown as the symbols, and were previously shown in figure 10(a). The solid and dashed curves correspond to the fit of a cubic spline to the data. The spline was used to calculate the derivatives used in the determination of the best coefficients for (3.8). The heavy-dotted curves result from the integration of (3.8). The initial amplitudes and Reynolds number correspond to the most-upstream data values. In this case we see an excellent agreement between the coupled amplitude model and the experimental data.

The comparison of the evolution equation (3.8) to the data with $\beta_H = -0.09$, Case 2, is shown in figure 11(b). These data were previously shown in figure 10(b). Again the agreement is excellent.

In both these comparisons, the correction to the linear growth for the mean flow divergence was included. We demonstrate that we cannot get these good results by any general fit, by not including the mean flow correction for the previous data. The result is shown in figure 11(c). This shows a very poor comparison to the original data. As we might expect, the error in neglecting the mean flow divergence was less pronounced, although still noticeable, in the lower adverse pressure gradient case (Case 1).

We want to emphasize that our goal was not to try 'any fit' but to base our general fit on a form which had a basis from first principles. Slight variations of the general form of these amplitude equations for subharmonic resonance in a Blasius boundary layer have previously been investigated in the same facility (Hsia 1993). These mainly involved the addition of nonlinear interaction terms such as A^2B and B^2A. These generally produced results with large excursions from the experimental development of a scale similar to those in figure 11(c). As we pointed out, the two coupled equations are extremely 'stiff' and slight differences in the amplitudes anywhere along their development have a large integrated effect downstream. Based on this, we believe that any ad hoc form of coupled model equations will not produce the good results produced by (3.8).

4. Discussion

As pointed out in the Introduction, this study was motivated in part by the need to predict if and where transition to turbulence would occur in adverse pressure gradient boundary layers in which the dominant primary instability mechanism is TS waves. These conditions are relevant to wings which are not highly swept. Upstream of the maximum thickness point, the favourable pressure gradient will

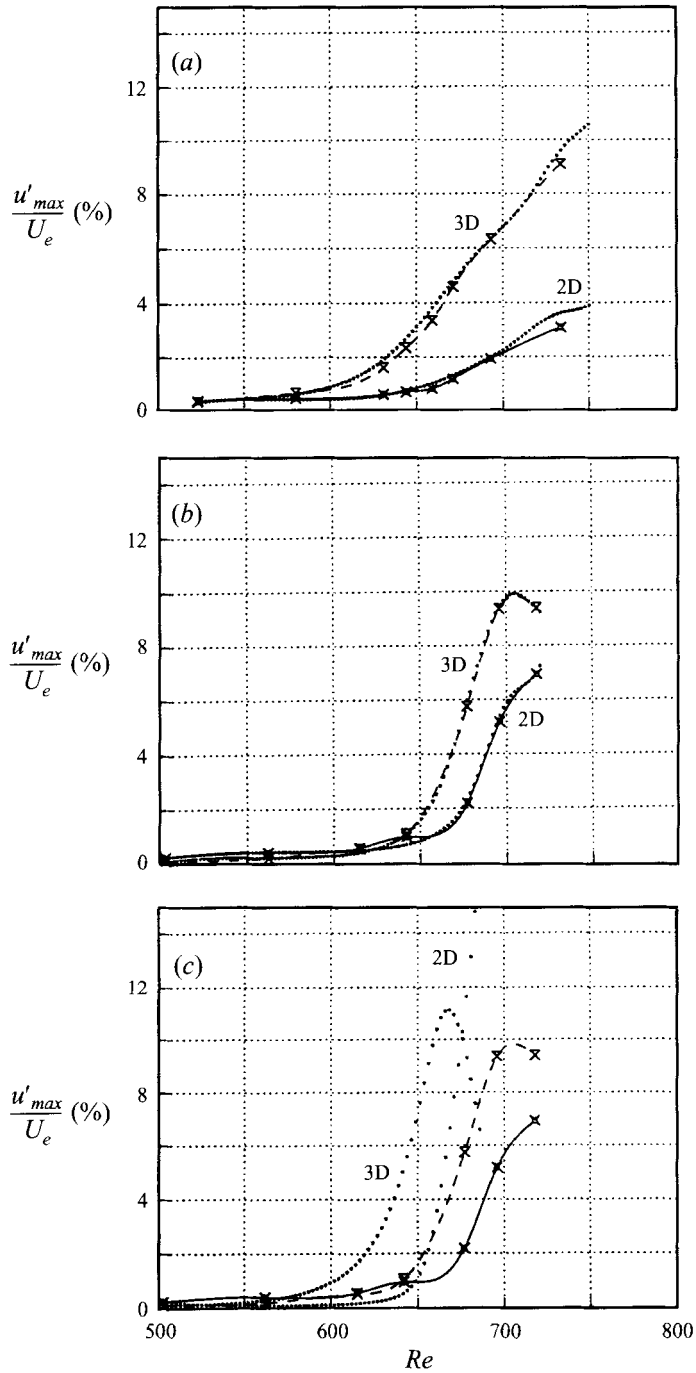

FIGURE 11. Streamwise development of maximum amplitude obtained from model equation (3.8). Symbols are original data. Dashed and solid curves are from a fit of a cubic spline to the data. The heavy-dotted curve is from integration of (3.8). (*a*) $\beta_H = -0.06$. (*b*) $\beta_H = -0.09$. Without correction for mean flow divergence in linear growth, (*c*) $\beta_H = -0.09$.

greatly suppress the growth of disturbances. Beyond this point, the reverse is the case. Here even a mild adverse gradient will greatly accelerate the growth of linear instability modes. With faster linear growth, nonlinear amplitudes will be reached more quickly. This will bring into play secondary instabilities, the most important of which results in the first growth of three-dimensional disturbances, which is an essential step to reaching a turbulent state. Correlation techniques such as e^N, which model only linear mechanisms, do not account for the nonlinear three-dimensional mode development. However, their use has continued because of their simplicity over numerical (Navier–Stokes) models. This is an important aspect when used as a tool for design. The amplitude models such as those developed by Goldstein & Lee (1992) and Mankbadi *et al.* (1993) are meant to be an alternative to numerical methods, which embody the nonlinear mechanisms, while retaining a degree of simplicity needed for design. The purpose of this work was to then compare the streamwise evolution of instability modes in an experiment with those predicted by the relevant amplitude models. Because the evolution is dependent on the initial conditions (amplitudes of the initial modes), these had to be known and well controlled in the experiment.

Overall, we found that the general form of the model equations (3.8) worked well and confirmed that they contain the proper physics for the sensitive coupled interaction present in three-dimensional mode subharmonic resonance. They indicated the importance of the mean flow divergence in the linear growth of the modes, and the quartic dependence of the fundamental mode amplitude on the subharmonic amplitude when the two modes become fully coupled.

In general there was a benefit in the use of the adverse pressure gradient boundary layer in testing the amplitude evolution model because we could more quickly reach the nonlinear stages while still maintaining low initial amplitudes. Compared to a Blasius layer, the adverse pressure gradient leads to faster linear growth of the plane TS mode. It therefore more quickly reaches amplitude levels which are large enough to produce the parametric resonance with the subharmonic oblique modes. This also occurs further upstream of Branch II so that the extended linear amplification of the TS mode leads to extra large amplitudes of the subharmonic. This in turn leads to a stronger back interaction from the subharmonic mode to the fundamental. As a result, the maximum amplitude reached by the fundamental mode is a significantly larger percentage of the maximum subharmonic amplitude than for the Blasius layer. For example for comparable initial conditions, in a Blasius flow the ratio $u'(f/2)_{max}/u'(f)_{max}$ was approximately 5 (Corke & Mangano 1989). In the present results with $\beta = -0.06$ the ratio was 2.9 and with $\beta = -0.09$ it was nearly unity (1.3).

With an adverse pressure gradient the analysis of Goldstein & Lee (1992) predicted that the amplitude evolution should exhibit an 'explosive' growth when the subharmonic mode amplitude reaches nonlinear levels. This entered through the cubic self-interaction term which caused a rapid increase in the instability growth, and ultimately lead to a singularity at a finite downstream position. In this context we did not see such an 'explosive' growth. However, the streamwise extent of amplitude saturation was extremely short compared to the Blasius layer. For example in figure 17 of Corke & Mangano (1989), the two most-amplified subharmonic resonance cases had a broad saturation region which was followed by a gradually decreasing amplitude which slowly merged into the turbulent state. In Cases 1 and 2 here, the extent to which the development of the modes could be followed ended with the most downstream points shown in the figure. Beyond those points, it was difficult to identify a spectral peak. On the basis of the spectra and the degree of unsteadiness

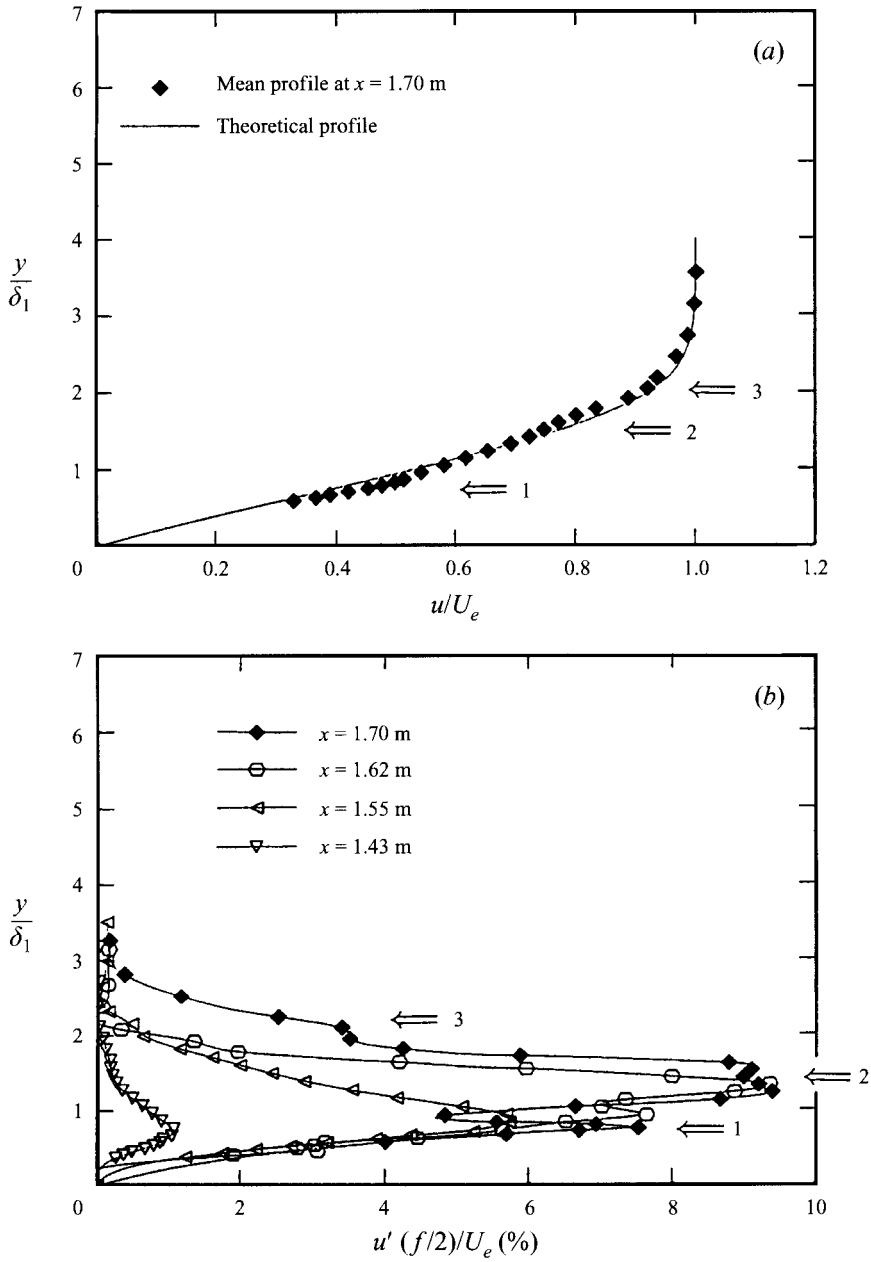

FIGURE 12. Mean velocity profile (*a*) and subharmonic mode amplitude distributions (*b*) with $\beta_H = -0.09$, Case 2.

in the time series, the flow looked turbulent. What is the origin of this different behaviour produced by the adverse pressure gradient?

As pointed out, the maximum amplitudes reached by the subharmonic mode in these two cases with adverse pressure gradient were twice as large as those in a Blasius layer with comparable initial conditions. As a result of these large amplitudes, the mean profile developed inflexions away from the wall. These are shown in figure 12(*a*). This corresponds to the last downstream position for $\beta_H = -0.09$. Shown in the figure

are the mean profile data points compared to the theoretical profile which is the solid curve. Upstream of this point, the measured mean profile collapsed well onto the theoretical profile, such as was shown for Case 1 in figure 4. In figure 12(*a*), three inflexion regions are identified and numbered. Label 1 denotes a change in the slope near the critical layer. This inflexion is a characteristic of subharmonic resonance. It results from the mean flow distortion when the subharmonic mode grows to large amplitude and has been observed in previous measurements in the same facility (Hsia 1993), and is predicted in the analysis of Mankbadi *et al.* 1993.

Labels 2 and 3 denote inflexions in the mean profile which are located away from the wall. Such high inflexions are never observed when the initial TS amplitudes are small. These are generally characteristic of a high-shear layer which is a feature of fundamental mode (K-type) transition. With K-type transition, the high-shear layer is caused by large initial two-dimensional mode amplitudes.

We observe a correspondence between the three labelled locations and peaks in the wall-normal amplitude distribution for the subharmonic mode shown in figure 12(*a*). The dominant peaks are at locations 1 and 2. Figure 12(*b*) shows the amplitude distributions for the last four measurement locations. The labelled peaks only appeared in the last two of these, and this coincided with the first appearance of the inflexions in the mean profile. A similar double-peaked distribution was also observed in the DNS-simulation of subharmonic-mode transition with the slightly larger adverse pressure gradient of $\beta_H = -0.1$, by Kloker & Fasel (1990).

We can get a further appreciation of the transition process for this case (Case 2) from the streamwise evolution of velocity time traces. Samples are shown in figure 13(*a*). These correspond to two R_x locations. The top trace is at $R_x = 677$, which is in the middle of the resonant growth region of the $f/2$ mode (figure 10). The bottom trace is at $R_x = 718$, which is at the end of the amplitude saturation region for the $f/2$ mode. The y-locations of these traces correspond to where u'/U_e is a maximum (figure 12*b*). These traces are a representative set of the total time series acquired in the experiment, and demonstrate the essential features we observe.

At the lower R_x location, the velocity time series is very regular. The dominant period corresponds to the subharmonic mode (19 Hz). These traces have not been phase averaged, so that strong periodicity exhibited in this trace is an example of the repeatability of one wave and the next. In the trace at the higher-R_x location, we still observe a large degree of periodicity, for example in the time interval from 0.3 to 0.45 s. However there are instances when higher frequencies appear in the velocity fluctuations, such as in the interval near $t = 0.25$ s. The appearance of these higher-frequency fluctuations, which are irregularly dispersed in the time series, suggests an additional instability of a thin, high-shear layer that we associate with the mean-profile inflexion. One can observe that this is different from what normally occurs in subharmonic mode transition in a Blasius boundary layer, by contrasting this time series with the equivalent location in figure 22(*d*) of Corke & Mangano (1989). There, higher and lower frequencies appear everywhere and uniformly in the velocity fluctuations. Corke & Mangano associated this with a frequency 'detuning' of the fundamental–subharmonic resonance (see also Corke 1995). The bellwether of this process is the appearance of dominant low-frequency components in the velocity spectra (e.g. figure 23(*d*) of Corke & Mangano). Velocity spectra in our case, corresponding to the x-location of the lower time trace at $R_x = 718$, are shown in figure 15(*b*). Here the spectral peaks corresponding to the f (38 Hz) and $f/2$ (19 Hz) modes are very large and well defined compared to the background fluctuations. The background fluctuation amplitude has grown

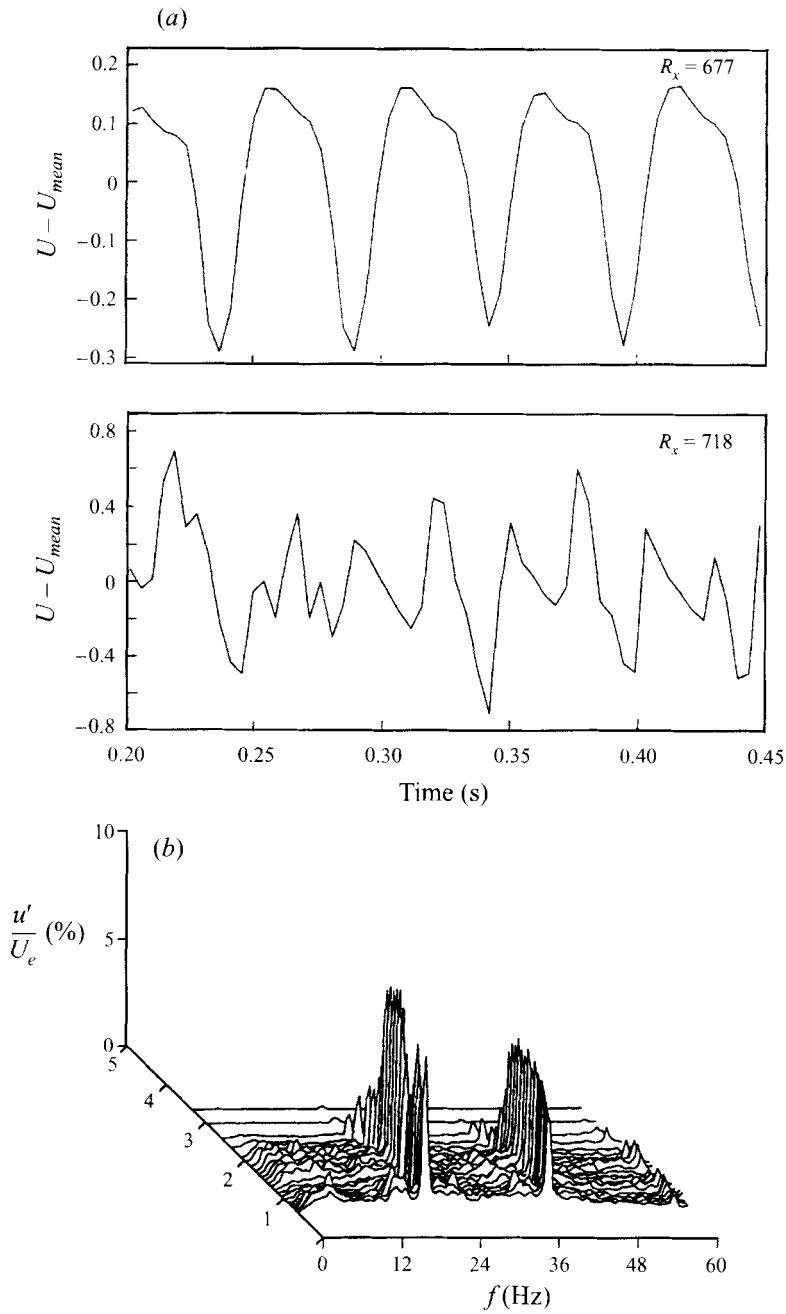

FIGURE 13. Sample velocity time traces (*a*) at two locations corresponding to $R_x = 677$ (top) and $R_x = 718$ (bottom), and velocity spectra (*b*) at different y-positions at $R_x = 718$, Case 2.

compared to upstream locations, for example seen in the spectra in figure 6, which is for Case 1, but is otherwise representative. In this case, the broadband results from the somewhat randomly occurring higher-frequency fluctuations seen in the downsteam time-trace. We do not observe in this case the dominant low-frequency modes we associate with the subharmonic transition in the zero pressure gradient flow.

The observation of the high-shear layer, which is not otherwise a general part of subharmonic mode transition, provides a short (inviscid) time scale for the last stage of transition to turbulence. This substantially shortens any energy saturation region compared to our previous experience in a Blasius boundary layer (Corke & Mangano 1989). With this we found a sharp transition from the coherent mode region to broadband fluctuations. This may be analogous to the 'explosive' growth at the end of the subharmonic mode development predicted by Goldstein & Lee (1992). In any event it is dramatically different from the behaviour with a zero pressure gradient and needs to be accounted for in transition prediction where adverse pressure gradients are present.

We want to acknowledge the useful discussions with Dr Reda Mankbadi and helpful comments of Dr Sang Soo Lee. This work was supported by a grant from NASA Lewis Research Center, No. NAG3-1519.

REFERENCES

Corke, T. C. 1995 Three-dimensional mode growth in boundary layers with tuned and detunded subharmonic resonance. *Phil. Trans. R. Soc. Lond.* A **352**, 453.

Corke, T. C. & Mangano, R. A. 1989 Resonant growth of three-dimensional modes in transitioning Blasius layers. *J. Fluid Mech.* **209**, 93.

Craik, A. D. D. 1971 Non-linear resonant instability in boundary layers. *J. Fluid Mech.* **50**, 393.

Goldstein, M. E. & Lee, S. S. 1992. Fully coupled resonant-triad interaction in an adverse-pressure-gradient boundary layer. *J. Fluid Mech.* **245**, 523.

Herbert, Th. 1983 Subharmonic three-dimensional disturbances in unstable plane shear flows. *AIAA Paper* 83-1759.

Herbert, Th. 1990 A code for linear stability analysis. In *Instability and Transition II* (ed. M. Hussaini & R. Voight), p. 121. Springer.

Herbert, Th. & Bertolotti, F. P. 1985 The effect of pressure gradients on the growth of subharmonic disturbances in boundary layers. In *Proc. Conf. Low Reynolds Number Airfoil Aerodyn.* (ed. T. Mueller), p. 65. Notre Dame University.

Hsia, Yu.-Ch. 1993 Amplitude ratio effects on 3-D mode resonance in boundary layers. MS thesis, Illinois Institute of Technology.

Kachanov, Yu. S. 1987 On the resonant nature of the breakdown of a laminar boundary layer. *J. Fluid Mech.* **184**, 43.

Kachanov, Yu. S., Koslov, V. V. & Levchenko, V. Ya. 1977 Nonlinear development of a wave in a boundary layer. *Fluid Dyn.* **12**, 383.

Kachanov, Yu. S. & Levchenko, V. Ya. 1984 The resonant interaction of disturbances at laminar-turbulent transition in a boundary layer. *J. Fluid Mech.* **138**, 209.

Kloker, M. 1993 Direkte numerische Simulation des laminar-turbulenten Stroemungsumschlages in einer stark verzoegerten Grenzschicht. Dissertation, University of Stuttgart, Germany.

Kloker, M. & Fasel, H. 1990 Numerical simulation of two- and three-dimensional instability waves in two-dimensional boundary layers with streamwise pressure gradient. In *Laminar-Turbulent Transition* (ed. D. Arnal & R. Michel), p. 681. Springer.

Korategere, S. S. 1990 Broad-band 3-D mode development in Blasius boundary layers by resonant mode detuning. MS thesis, Illinois Institute of Technology.

Mankbadi, R. R. 1990 Critical layer nonlinearity in the resonance growth of three dimensional waves in boundary layer. *NASA TM*-103639.

Mankbadi, R. R. 1991 Asymptotic analysis of boundary-layer transition. *Fourth Int. Symp. on CFD.*

Mankbadi, R. R., Wu, X. S. & Lee, S. S. 1993 A critical-layer analysis of the resonant triad in boundary-layer transition: nonlinear interactions. *J. Fluid Mech.* **256**, 85.

Saric, W. S. & Thomas, A. S. W. 1984 Experiments on the subharmonic route to turbulence in boundary layers. In *Proc. IUTAM Symp. on Turbulence and Chaotic Phenomena in Fluids, Kyoto, Japan.*

VAN INGEN, J. L. 1956 A suggested semi-empirical method for calculation of the boundary layer transition region. *Rep.* UTH1-74 University of Technology, Dept. Aero. Engng.

ZELMAN, M. B. & MASLENNIKOVA, I. I. 1993*a* Tollmien–Schlichting-wave resonant mechanism for subharmonic-type transition. *J. Fluid Mech.* **252**, 449.

ZELMAN, M. B. & MASLENNIKOVA, I. I. 1993*b*. Subharmonic transition spectra generation and transition prediction in boundary layers. *Eur. J. Mech.* B/*Fluids* **12**, 161.